Phys Chem Minerals (2003) 30: 570–581
DOI 10.1007/s00269-003-0348-9

ORIGINAL PAPER

F. Cámara · R. Oberti · G. Iezzi · G. Della Ventura

The $P2_1/m \leftrightarrow C2/m$ phase transition in synthetic amphibole Na NaMg Mg_5 Si_8 O_{22} $(OH)_2$: thermodynamic and crystal-chemical evaluation

Received: 17 March 2003 / Accepted: 1 July 2003

Abstract The $P2_1/m \leftrightarrow C2/m$ displacive phase transition in the synthetic end-member amphibole Na NaMg Mg_5 Si_8 O_{22} $(OH)_2$ has been studied by monitoring changes in unit-cell parameters and the intensities of superlattice reflections at 25–400 °C. This amphibole allows investigation of the effects of compositional variations at the A- and B-group sites upon the transition. Polynomial fitting of a 24 Landau potential to the evolution of the order parameter with T yielded a T_c of 257 ± 3 °C, and Landau coefficients compatible with a second-order transition. Structure refinement of single-crystal data collected at 25, 140, 270 and 370 °C allowed modelling of the structural changes as a function of T and symmetry. Crystal-chemical analysis suggests that differences in T_c in cummingtonites and in the crystal of this work depend mainly upon the relations between the aggregate ionic radii of the B- and C-group cations.
Electronic Supplementary Material of Table 5 is available in the online version of this article at http://dx.doi.org/10.1007/s00269-003-0348-9

Keywords Amphibole · H*T*-XRD · Displacive phase transition · Synthesis

F. Cámara (✉) · R. Oberti
CNR-Istituto di Geoscienze e Georisorse,
sezione di Pavia, via Ferrata 1, 27100 Pavia, Italy
e-mail: camara@crystal.unipv.it
Tel: +39-0382-505867
Fax: +39-0382-505887

G. Iezzi
Dipartimento di Scienze della Terra,
Università G. D'Annunzio, 66013 Chieti Scalo, Italy

G. Iezzi
Bayerisches Geoinstitut, Universität Bayreuth,
95440 Bayreuth, Germany

G. Della Ventura
Dipartimento di Scienze Geologiche, Università di Roma Tre,
Largo S. Leonardo Murialdo 1, 00146 Rome, Italy

Introduction

Along the cummingtonite–grunerite series, where cummingtonite refers to the fraction of the solid solution □ $(Mg,Fe^{2+},Mn,Li)_2$ Mg_5 Si_8 O_{22} $(OH)_2$ with Li < 1.0 and Mg ≥ 0.5 atoms per formula unit (apfu) and grunerite to that with Li < 1.0 and Mg < 0.5 apfu (Leake et al. 1997), Mg-rich compositions have $P2_1/m$ symmetry, whereas Fe-richer compositions have $C2/m$ symmetry. The reversible displacive $P2_1/m \leftrightarrow C2/m$ phase transition occurs as a function of changes in either pressure (P), temperature (T) or composition (X). The transition behaviour as a function of T has been studied in different cummingtonitic compositions by Yang and Smyth (1996), and in manganocummingtonite by Prewitt et al. (1970), Sueno et al. (1972) and Reece et al. (2000). Studies as a function of P in cummingtonites have been reported by Zhang et al. (1992), Yang et al. (1998) and Boffa Ballaran et al. (2000). All these studies concluded that the $P2_1/m \leftrightarrow C2/m$ phase transition is mainly controlled by the aggregate ionic radius, $\langle r_{M4} \rangle$, at the M4 site, which in turn is a function of the B-site composition.

The $C2/m$ symmetry is stabilized by the presence of larger cations, such as Fe^{2+} and Mn^{2+}, at the M4 site. However, the M4 composition depends both on the overall chemistry of the investigated amphibole (Hirschmann et al. 1994; Yang and Hirschmann 1995) and on non-convergent order–disorder between the B- and C-group sites which occurs during annealing above ~400 °C for Fe^{2+} (Ghose and Weidner 1972) and ~550 °C for Mn^{2+} (Reece et al. 2000). In any case, the overall fraction of larger dominant cation [e.g. $X_{Fe} = Fe/(Mg + Mn + Fe)$] can be used as a useful indicator. At room pressure, the $P2_1/m$ structure is stable up to $X_{Fe} = 0.38$ (Hirschmann et al. 1994) or $X_{Mn} = 0.29$ (Ghose and Yang 1989). Boffa Ballaran et al. (2001) carried out a room-T study of cummingtonites equilibrated at 700 °C and then quenched, and concluded that $X_{Fe} = 0.57(1)$ is the critical composition under which the

$P2_1/m$ phase is stable under these conditions. Decreasing X_{Fe} decreases the transition pressure P_c (Yang et al. 1998; Boffa Ballaran et al. 2000).

The available data confirm second-order (or close to second-order) character for both the $C2/m \rightarrow P2_1/m$ phase transition occurring with increasing pressure (Boffa Ballaran et al. 2000) and the $P2_1/m \rightarrow C2/m$ phase transition occurring with increasing temperature (Reece et al. 2000) as well as with increasing X_{Fe}. The critical temperature and the critical pressure are proportional to X_{Fe} at both the microscopic and macroscopic scales (Yang et al. 1998; Boffa Ballaran et al. 2001, 2002).

The space group $P2_1/m$ in amphiboles is rare; besides for cummingtonites, it has been reported for a synthetic amphibole for which combination of electron- and ion-probe analysis and of single-crystal-structure refinement suggested a crystal-chemical formula $Na_{0.95}(Na_{0.64}Mg_{0.97}Li_{0.27}H_{0.12})Mg_5Si_8O_{22}(OH)_2$, and thus an excess OH located at the M4 site (Oberti et al. 2000). Recent experiments under different P and T conditions (Iezzi et al. 2003) showed that samples varying from $Na_1Na_1Mg_1Mg_5Si_8O_{22}(OH)_2$ ($T = 750$ °C, $P = 4$ kbar) to $Na_{0.81}Na_{0.81}Mg_{1.19}Mg_5Si_8O_{22}(OH)_2$ ($T = 900$ °C, $P = 5$ kbar) all have $P2_1/m$ symmetry under ambient conditions. This system is significantly different from cummingtonite for two main reasons: (1) the A-group sites are nearly fully occupied, and (2) the absence of Fe^{2+} avoids the complication of Mg/Fe ordering between the B- and C-group sites. Therefore, this composition provides an excellent opportunity to evaluate how the aggregate ionic radius and ionic charge at M4 affect the critical transition temperature (T_c), and whether or not the A-site cation affects T_c and the macroscopic strain.

Experimental methods

Synthesis

For the present work, a crystal of suitable size and quality was hand-picked from run-powder 334, crystallized at 900 °C and 5 kbar by Iezzi et al. (2003). The starting product was prepared by blending in stoichiometric amounts dry oxide mixtures, and hydrothermal synthesis was done in internally heated pressure vessels at the Institut für Mineralogie of the Universität Hannover. Full details for the experimental procedures are given in Iezzi et al. (2003). EMP analysis coupled with room-T structure refinement gave the following unit formula for the studied crystal (Iezzi et al. 2003): $Na_{0.81}Na_{0.81}Mg_{1.19}Mg_5Si_8O_{22}(OH)_2$. This sample is very close to the nominal Na NaMg $Mg_5Si_8O_{22}(OH)_2$ end-member stoichiometry, the only departure being a loss of Na and an increase in Mg, according to the $^{A}\square_1{}^{B}Mg_1{}^{A}Na_{-1}{}^{B}Na_{-1}$ exchange vector.

High-temperature X-ray single-crystal diffraction

Intensity and unit-cell data were collected at room temperature at CNR-IGG-PV using a Bruker AXS D8 single-crystal diffractometer equipped with a SMART Apex CCD detector and working with graphite-monochromatized Mo$K\alpha$ X-radiation at 55 kV and 30 mA; the crystal-to-detector distance was 4.0 cm. Three-dimensional data were integrated and corrected for Lorentz, polarization and background effects using the SAINT+ software version 6.02 (Bruker AXS). Unit-cell dimensions were calculated from least-squares refinement of the positions of all the collected reflections. The unweighted full-matrix least-squares refinement on F was done with a CNR-IGG-PV program written specifically to deal with complex solid solutions (Cannillo E., personal communication). The occupancies of the M1, M2 and M3 sites were first refined (maximum deviation from complete Mg occupancy $< \pm$ 1%) and then fixed to Mg = 1 in the final cycles. Scattering curves for fully ionized chemical species were used at all cation sites except the T sites, neutral vs. ionized scattering curves were used at the T and anion sites (cf. Hawthorne et al. 1995 and references therein for more detail).

In situ annealing was done using a microfurnace specifically built for the Philips PW1100 four-circle diffractometer at the Department of Earth Sciences of the University of Cambridge. This furnace allows working at temperatures up to 1100 °C and data collection in the 2θ range 3–58°. The crystal was put in a quartz vial (0.2 mm ∅), and kept steady by quartz wool, which also avoids mechanical stress. Graphite-monochromatized Mo $K\alpha$ X-radiation and working conditions of 55 kV and 30 mA were used for crystal analysis and data collection.

After each annealing step (10 °C), lattice parameters were measured by centering 24 selected hkl a-type reflections ($h + k = 2n$). The intensities of six hkl b-type reflections ($h + k = 2n + 1$) (namely, $\bar{1}04$, $\bar{3}6\bar{5}$, $\bar{1}63$, 144, 161, 502) were monitored at each step (ω-rotations and step-scan profiles recorded with a scan width of 3°), and scaled with respect to those of adjacent a-type reflections in the same reciprocal row ($\bar{2}04$, $\bar{4}6\bar{5}$, $\bar{2}63$, $\bar{2}44$, 151, 602). This procedure allowed detection of the temperature of transition via a careful inspection of the intensity of b-type reflections and of the shape of their profiles (see below). Three further data collections were done before and after the transition temperature to monitor changes in all the structural parameters. Owing to the presence of the furnace, the maximum θ for these data collections is limited to 27°. Profiles were integrated following the method of Lehmann and Larsen (1974) modified by Blessing et al. (1974). Intensities were corrected for Lorentz and polarization factors, and for absorption using ψ scans (North et al. 1968). Structure refinements were made with the same procedure described before at $T = 270$ and 370 °C. For the $P2_1/m$ data set collected at 140 °C, in which most of the b-type reflections were very weak, it was necessary to do a weighted refinement on all the reflections, and a weighting scheme similar to that used in the program SHELXL-97 (Sheldrick 1997) was adopted.

Selected crystal data and refinement information for the various data collections are given in Table 1. Atom positions and displacement parameters are given in Table 2, and selected interatomic distances and angles are given in Table 3. Unit-cell parameters, $\Sigma I_b/\Sigma I_a$, and the related principal components of the strain tensor measured at each annealing step are given in Table 4. Observed and calculated structure factors are reported in Table 5 (deposited).

Results

Transition temperature, T_c

Landau theory is commonly used to describe displacive phase transitions (cf. Dove 1997 for a useful overview). A proper Landau expansion in one order parameter with second; fourth- and sixth-order terms (246 potential)

$$G = \frac{1}{2}a_D(T - T_c)Q_D^2 + \frac{1}{4}b_DQ_D^4 + \frac{1}{6}c_DQ_D^6 \quad , \qquad (1)$$

Table 1 Selected crystal and refinement data for crystal 334 no. 1 at different T

IGG code	Room T ibw	140 °C idl	270 °C idg	370 °C idm
a (Å)	9.685(1)	9.706(2)	9.723(2)	9.737(1)
b (Å)	17.920(2)	17.986(3)	18.027(3)	18.049(3)
c (Å)	5.268(1)	5.286(1)	5.301(1)	5.303(1)
β (°)	102.44(3)	102.37(1)	102.26(1)	102.22(1)
V (Å^3)	892.8	901.4	907.9	910.9
Space group	$P2_1/m$	$P2_1/m$	$C2/m$	$C2/m$
θ range (°)	2–35	2–26	2–27	2–26
Threshold cut	3 σ(I)	0 σ(I)	2 σ(I)	2 σ(I)
No. all	4037	1850	993	928
No. obs	2946	1850	491	456
R sym × 100	3.7	11.5	7.9	7.9
R obs × 100	4.0	[5.9 for >2 σ(I)]	4.3	4.2
R all × 100	5.9	7.9	13.3	13.1

where a, b and c are Landau coefficients and Q_D is the order parameter, can be used to derive the dependence of $Q_D{}^2$ on T. A simpler 24 Landau potential can also be used:

$$G = \frac{1}{2}a_D(T - T_c)Q_D^2 + \frac{1}{4}b_D Q_D^4 \quad . \tag{2}$$

According to Carpenter et al. (1990), the order parameter Q_D is proportional to the aggregate intensity ratio, $\Sigma I_b/\Sigma I_a$, where I_b are the intensities of reflections with $h + k = 2n + 1$ (b-type) and I_a the intensities of the reflections with $h + k = 2n$ (a-type). Therefore both the character of the phase transition and the T_c value can be obtained following the evolution of $\Sigma I_b/\Sigma I_a$ as a function of temperature.

Our data on crystal 334 no. 1 show that $\Sigma I_b/\Sigma I_a$ continuously decreases from room T to ~250 °C (Fig. 1). Beyond this value, b-type reflections are no longer detectable, and the crystal has $C2/m$ symmetry. Repeated heating and cooling cycles showed the same behaviour; no hysteresis was detected.

Substituting Q_D^2 with $\Sigma I_b/\Sigma I_a$ in Eq. (1), we can calculate T_c from the measured evolution of superlattice reflections from a polynomial fit of:

$$T = T_c + \frac{b_D}{a_D}\left(\sum I_b \Big/ \sum I_a\right) + \frac{c_D}{a_D}\left(\sum I_b \Big/ \sum I_a\right)^2 \quad . \tag{3}$$

The data measured in the T range 25–250 °C gave a calculated T_c of 525 ± 3 K, and values of −832 ± 49 K and −459 ± 197 K for the b_D/a_D and c_D/a_D terms, respectively. In the simplified 24 Landau treatment, T_c can be obtained by a linear fit to:

$$T = T_c + \frac{b_D}{a_D}\left(\sum I_b \Big/ \sum I_a\right) \quad , \tag{4}$$

which yielded $T_c = 530 \pm 2$ K, and $b_D/a_D = -943 \pm 14$ K. The larger uncertainties obtained for the b_D/a_D and c_D/a_D coefficients with the polynomial fit in theory do not justify the use of a 246 Landau expansion. However, the results of this treatment are provided for two reasons: the first is to allow straightforward comparison with previous literature, and the second is that previous studies (Boffa Ballaran et al. 2000) showed evidence of tricritical behaviour in sample Y42XB with $X_{Al+Na+Ca} = 0.32$, with 0.03 apfu Na at the A-site. In any case, the present results are compatible with second-order character for the $P2_1/m \leftrightarrow C2/m$ phase transition in Na NaMg Mg_5 Si_8 O_{22} $(OH)_2$.

Lattice parameters and strain calculations

The evolution of the unit-cell parameters as a function of T is shown in Fig. 2a–e. All unit-cell edges lengthen with increasing T, but the expansion rates change at the phase transition, particularly for the c edge. The b and c edges are shorter in the $P2_1/m$ symmetry than expected by extrapolation of the high-T $C2/m$ symmetry, whereas a is longer. The β angle decreases with increasing T, but the rate of decrease reduces significantly around T_c. All these features confirm that the phase transition concerns primarily the double chains of tetrahedra (whose stretching correlates with the c-edge behaviour), as well as their matching requirements with the strip of octahedra (which correlate with the β angle). This behaviour is consistent with the fact that in $P2_1/m$ amphibole structure there are two independent double chains, while there is only one in $C2/m$ structure, and only one independent set of M sites. A similar behaviour is also shown by the unit-cell parameters reported by Reece et al. (2000) in their in situ high-T neutron powder-diffraction study of manganocummingtonite.

Yang et al. (1998) reported variations in unit-cell parameters as a function of increasing P for a cummingtonite with $X_{Fe} = 0.50$, and Boffa Ballaran et al. (2000) for four cummingtonites with $X_{Fe} = 0.45$, 0.69, 0.89 and 0.97. The P_c values were found to increase with X_{Fe} (0.7, 1.57, 2.7 and 2.77 GPa, respectively), and the relative changes of the unit-cell edges in the two symmetries are analogous to those reported in this work and in Reece et al. (2000), whereas the β angle is smaller in the $P2_1/m$ space group than expected by extrapolation of the $C2/m$ values.

Table 2a Crystal 334 no. 1 $P2_1/m$ symmetry. Room temperature (*first row*) and 140 °C (*second row*)

Site	x/a	y/b	z/c	B_{eq}	β_{11}	β_{22}	β_{33}	β_{12}	β_{13}	β_{23}
O1A	−0.1368(2)	0.3365(1)	0.1970(3)	0.59	19(2)	5(1)	48(5)	−1(1)	7(2)	−2(1)
	−0.1388(9)	0.3357(5)	0.1957(15)							
O1B	0.3629(2)	0.8367(1)	0.2257(3)	0.58	18(2)	5(1)	46(5)	0(1)	6(2)	0(1)
	0.3651(9)	0.8370(5)	0.2278(15)							
O2A	−0.1300(2)	0.4215(1)	0.7021(3)	0.72	18(2)	7(1)	62(5)	−1(1)	10(2)	−5(1)
	−0.1278(9)	0.4211(5)	0.7126(16)							
O2B	0.3735(2)	0.9219(1)	0.7355(3)	0.77	25(2)	7(1)	50(5)	−1(1)	8(2)	−3(1)
	0.3701(10)	0.9216(6)	0.7263(16)							
O3A	−0.1398(3)	1/4	0.6937(4)	0.68	22(2)	5(1)	58(7)	0	7(3)	0
	−0.1361(12)		0.6983(22)							
O3B	0.3576(3)	3/4	0.7219(5)	0.71	17(2)	6(1)	71(7)	0	9(3)	0
	0.3551(12)		0.7236(22)							
O4A	0.1199(2)	0.4990(1)	0.7951(4)	1.08	42(2)	5(1)	93(6)	−6(1)	−7(2)	−2(1)
	0.1246(10)	0.4986(5)	0.7891(17)							
O4B	0.6260(3)	0.9938(1)	0.7662(4)	1.86	66(3)	11(1)	127(7)	−17(1)	−39(3)	18(2)
	0.6204(11)	0.9947(5)	0.7724(18)							
O5A	0.0965(2)	0.3676(1)	0.0237(3)	0.95	24(2)	10(1)	74(5)	1(1)	13(2)	12(1)
	0.0961(8)	0.3692(4)	0.0319(14)							
O5B	0.6000(2)	0.8852(1)	0.0970(3)	0.90	23(2)	8(1)	76(5)	−2(1)	9(2)	9(1)
	0.5987(8)	0.8833(4)	0.0878(15)							
O6A	0.0996(2)	0.3802(1)	0.5269(3)	1.00	23(2)	10(1)	82(5)	3(1)	0(2)	−17(1)
	0.0985(8)	0.8833(4)	0.0878(15)							
O6B	0.5928(2)	0.8578(1)	0.5969(3)	1.01	23(2)	12(1)	59(5)	2(1)	3(2)	−11(1)
	0.5943(8)	0.8586(4)	0.5877(14)							
O7A	0.0922(3)	1/4	0.3006(5)	0.86	24(2)	4(1)	116(8)	0	12(3)	0
	0.0942(13)		0.3001(22)							
O7B	0.5896(3)	3/4	0.2607(5)	0.87	21(2)	4(1)	136(8)	0	19(3)	0
	0.5869(12)		0.2608(23)							
T1A	0.0324(1)	0.3355(1)	0.2616(1)	0.50	17(1)	4(1)	43(2)	−1(1)	5(1)	−1(1)
	0.0323(4)	0.3359(2)	0.2645(6)							
T1B	0.5320(1)	0.8344(1)	0.2951(1)	0.49	17(1)	4(1)	37(2)	0(1)	6(1)	1(1)
	0.5306(4)	0.8343(2)	0.2894(6)							
T2A	0.0407(1)	0.4215(1)	0.7678(1)	0.52	17(1)	4(1)	41(2)	−1(1)	5(1)	−1(1)
	0.0401(4)	0.4216(2)	0.7722(6)							
T2B	0.5441(1)	0.9195(1)	0.7991(1)	0.60	20(1)	5(1)	46(2)	−3(1)	4(1)	2(1)
	0.5446(4)	0.9195(2)	0.7963(6)							
M1	−0.2500(1)	0.3382(1)	0.4847(1)	0.64	23(1)	5(1)	48(2)	0(1)	8(1)	−1(1)
	−0.2485(6)	0.3382(1)	0.4908(9)							
M2	−0.2501(1)	0.4295(1)	0.9838(2)	0.65	21(1)	4(1)	63(2)	0(1)	10(1)	2(1)
	−0.2503(6)	0.4296(2)	0.9829(9)							
M3	−0.2496(1)	1/4	0.9858(2)	0.61	21(1)	4(1)	50(3)	0	4(1)	0
	−0.2533(8)		0.9898(13)							
M4	−0.2468(2)	0.5065(1)	0.4812(3)	0.80	24(1)	7(1)	72(5)	0(1)	27(2)	2(1)
	−0.2406(9)	0.5059(3)	0.4925(16)							
A	0.2658(3)	1/4	0.0456(7)	3.83	63(3)	44(1)	414(15)	0	130(6)	0
	0.2707(12)		0.0444(24)							
M4′	−0.2606(3)	0.5209(1)	0.4797(5)	1.46						
	−0.2593(15)	0.5228(5)	0.4710(26)							
H1	−0.056(7)	1/4	0.727(13)	3.86						
H2	0.561(6)	1/4	0.246(13)	2.21						

The components of the macroscopic spontaneous strain accompanying the $P2_1/m \leftrightarrow C2/m$ transition are (Carpenter et al. 1998):

$$e_{11} = \frac{a}{a_0} - 1 \tag{5}$$

$$e_{22} = \frac{b}{b_0} - 1 \tag{6}$$

$$e_{33} = \frac{c \sin\beta}{c_0 \cos\beta_0} - 1 \tag{7}$$

$$e_{12} = e_{23} = e_{21} = e_{32} = 0 \tag{8}$$

$$e_{13} = e_{31} = \frac{1}{2}\left(\frac{c\cos\beta}{c_0 \sin\beta_0} - \frac{a\cos\beta_0}{c_0 \sin\beta_0}\right) , \tag{9}$$

where the reference parameters, a_0, b_0, c_0, β_0, are those of a hypothetical structure with $Q_D = 0$. The volume strain V_s is given by

$$V_s = \frac{V}{V_0} - 1 \ . \tag{10}$$

The values of the reference parameters, a_0, b_0, c_0, β_0 and V_0, can be obtained by linear regression of the values measured for a, b, c, $\sin\beta$ and V at $T > 260$ °C (Table 4;

Table 2b Crystal 334 no. 1. *C*2/*m* symnmetry. Structure refinement at 270 °C (*first row*) and 370 °C (*second row*)

Site	*x*/*a*	*y*/*b*	*z*/*c*	*B eq*	β_{11}	β_{22}	β_{33}	β_{12}	β_{13}	β_{23}
O1	0.1126(6)	0.0863(3)	0.2117(13)	0.86	16(6)	9(2)	80(28)	−3(3)	12(10)	1(5)
	0.1133(7)	0.0862(3)	0.2098(12)	0.93	20(8)	9(2)	102(28)	0(3)	36(10)	−1(5)
O2	0.1221(7)	0.1718(3)	0.7191(13)	1.14	41(7)	11(2)	55(26)	−4(3)	19(12)	1(5)
	0.1218(8)	0.1722(3)	0.7198(13)	1.44	52(9)	11(3)	71(26)	−5(3)	−20(13)	−5(6)
O3	0.1088(9)	0	0.7058(20)	1.10	30(6)	7(3)	119(45)	0	14(17)	0
	0.1090(11)	0	0.7091(22)	1.79	57(14)	6(3)	225(56)	0	22(22)	0
O4	0.3714(8)	0.2469(3)	0.7798(19)	1.80	52(9)	11(2)	162(38)	−12(3)	−19(14)	4(6)
	0.3728(10)	0.2467(4)	0.7846(19)	2.04	69(12)	15(2)	128(38)	−12(4)	−8(15)	6(6)
O5	0.3467(8)	0.1266(4)	0.0588(13)	1.56	38(8)	18(2)	105(25)	1(3)	28(11)	24(6)
	0.3466(9)	0.1263(4)	0.0572(13)	1.85	56(9)	21(2)	83(27)	−1(3)	29(13)	26(6)
O6	0.3456(7)	0.1191(4)	0.5591(12)	1.70	32(8)	24(2)	58(2)	6(3)	−7(11)	−29(6)
	0.3445(8)	0.1193(4)	0.5583(14)	1.98	32(8)	25(3)	143(3)	5(3)	10(13)	−29(7)
O7	0.3393(11)	0	0.2782(22)	1.64	59(11)	4(2)	230(45)	0	49(18)	0
	0.3389(12)	0	0.2558(24)	1.70	31(12)	11(3)	245(49)	0	26(19)	0
T1	0.2810(3)	0.0850(1)	0.2759(5)	0.65	25(3)	5(1)	38(9)	2(1)	14(4)	0(2)
	0.2812(3)	0.0850(1)	0.2756(5)	0.80	23(3)	8(1)	56(9)	−1(1)	12(4)	1(2)
T2	0.2924(3)	0.1707(1)	0.7833(6)	0.84	23(2)	7(1)	75(9)	−2(1)	9(4)	3(2)
	0.2917(3)	0.1707(1)	0.7826(6)	0.97	37(3)	7(1)	67(9)	−3(1)	13(4)	1(2)
M1	0	0.0883(2)	1/2	0.85	31(5)	10(1)	22(17)	0	20(7)	0
	0	0.0882(2)	1/2	1.14	49(6)	12(2)	35(17)	0	41(8)	0
M2	0	0.1795(2)	0	1.11	38(5)	6(1)	114(19)	0	22(8)	0
	0	0.1801(3)	0	1.37	35(5)	9(1)	151(19)	0	12(9)	0
M3	0	0	0	0.87	17(6)	4(2)	117(32)	0	−13(12)	0
	0	0	0	1.59	53(9)	3(2)	207(34)	0	1(15)	0
M4	0	0.2620(4)	1/2	2.54	78(9)	30(3)	133(32)	0	85(13)	0
	0	0.2617(4)	1/2	2.36	58(9)	31(3)	127(29)	0	76(13)	0
A	0	1/2	0	2.27	27(35)	41(14)	27(13)	0	−22(51)	0
	0	1/2	0	2.64	45(44)	43(15)	31(125)	0	−28(57)	0
A*m*	0.0259(28)	1/2	0.0914(48)	2.76	50(37)	36(8)	213(116)	0	71(54)	0
	0.0340(31)	1/2	0.1132(52)	3.21	70(36)	41(9)	144(105)	0	2(49)	0
H	0.195(10)	0	0.767(20)	0.01						
	0.177(15)	0	0.733(27)	2.84						

Fig. 2). When T is the absolute temperature (K), the results are:

$$a_0(\text{Å}) = 9.6493(53) + 0.000137(9) \cdot T \qquad (R = 0.97)$$
$$b_0(\text{Å}) = 17.923(16) + 0.000197(25) \cdot T \qquad (R = 0.90)$$
$$c_0(\text{Å}) = 5.2815(34) + 0.0000358(56) \cdot T \qquad (R = 0.87)$$
$$\sin\beta_0 = 0.97610(13) - 0.00000196(21) \cdot T \qquad (R = 0.93)$$
$$V_0(\text{Å}^3) = 891.5(1.1) + 0.0307(18) \cdot T \qquad (R = 0.98),$$

where a number of digits higher than the esd is given to limit rounding errors.

Individual strain parameters were calculated according to Eqs. (5–10), and the results are shown in Fig. 3a. The total scalar strain $\varepsilon_{ss} = \sqrt{\sum_{i,k} e_{ik}^2}$ at room T is ~0.004(1). The uncertainties on strain components mainly depend on those on unit-cell parameters. The software used at CNR-IGG Pavia to derive and refine unit-cell parameters from the positions of diffraction peaks propagates uncertainties in a highly "pessimistic" way in order to take into account all the possible experimental factors included the centering of the crystal. The dependence of the strain components and volume strain observed in Fig. 3a is compatible with a linear variation, albeit some evidence – somewhat concealed by the uncertainties – might suggest a more tricritical behaviour.

The coupling between the individual strain components and the order parameter is expected to be of the form $\lambda e_{ik} Q_D^2$, with $i,k = 1$–3, for a coelastic phase transition (Carpenter et al. 1998). Strain components scale approximately with $\Sigma I_b/\Sigma I_a$, yielding $\lambda = 0.0156(9)$ (Fig. 3b). This value is larger than those calculated for the H*P* transition in cummingtonites by Boffa-Ballaran et al. (2000), which range from 0.0006 to 0.0134. A direct comparison of the λ values might, however, be biased by a different choice of *a*-type and *b*-type reflections. The subset used for cummingtonites has not been specified, but its choice was certainly more limited in H*P* experiments because of the hindrance of the experimental setting.

Boffa Ballaran et al. (2000) found that the strain components for the H*P* $P2_1/m \rightarrow C2/m$ transitions were smaller in sample Y42XB ($X_{Al+Na+Ca} = 0.32$, with 0.03 apfu Na at the A site), and suggested that the "exotic" cations affect the coupling coefficient and/or the elastic constants. Accordingly, even smaller values were obtained for crystal 334 no. 1, which has a higher Na content. Reece et al. (2000) reported even smaller spontaneous scalar strain for the H*T* $P2_1/m \rightarrow C2/m$ phase transition in manganoan cummingtonite with $^{[M4]}(Na_{0.13}Ca_{0.41}Mg_{0.46}Mn_{1.00})$. However, their data could be slightly biased by the low T_c, 107 °C, which did not allow them to constrain the calculation.

Table 3 Selected interatomic distances (Å) and angles (°) for crystal 334 no. 1 at different T and symmetries. *r.m.* means distances corrected for rigid motion (Busing and Levy 1964)

$P2_1/m$		Room T	r.m.	140 °C	$C2/m$		270 °C	r.m.	370 °C	r.m.
T1A–O1A		1.600(2)	1.608	1.622(9)	T1–O1		1.600(6)	1.604	1.598(7)	1.600
–O5A		1.618(2)	1.624	1.607(8)	–O5		1.614(7)	1.625	1.617(7)	1.630
–O6A		1.620(2)	1.626	1.624(8)	–O6		1.621(7)	1.634	1.619(7)	1.632
–O7A		1.636(1)	1.640	1.654(5)	–O7		1.634(42)	1.645	1.633(5)	1.643
< T1A–O >		1.619	1.624	1.627	< T1–O >		1.617	1.627	1.617	1.626
T1B–O1B		1.600(2)	1.601	1.570(8)						
–O5B		1.627(2)	1.631	1.629(8)						
–O6B		1.627(2)	1.632	1.626(8)						
–O7B		1.636(1)	1.641	1.630(5)						
< T1B–O >		1.623	1.626	1.614						
T2A–O2A		1.615(2)	1.617	1.592(9)	T2–O2		1.618(7)	1.619	1.617(8)	1.620
–O4A		1.578(2)	1.584	1.602(9)	–O4		1.576(7)	1.587	1.582(8)	1.592
–O5A		1.652(2)	1.657	1.658(8)	–O5		1.648(7)	1.657	1.649(7)	1.660
–O6A		1.672(2)	1.677	1.677(8)	–O6		1.675(7)	1.686	1.673(7)	1.684
< T2A–O >		1.629	1.634	1.632	< T2–O >		1.629	1.637	1.630	1.639
T2B–O2B		1.614(2)	1.615	1.655(10)						
–O4B		1.577(2)	1.591	1.557(9)						
–O5B		1.663(2)	1.666	1.652(8)						
–O6B		1.672(2)	1.677	1.696(8)						
< T2B–O >		1.632	1.637	1.640						
M1–O1A		2.054(2)	2.054	2.069(10)	M1–O1	x 2	2.060(7)	2.062	2.075(6)	2.077
–O1B		2.059(2)	2.060	2.053(10)	–O2	x 2	2.107(7)	2.110	2.116(7)	2.120
–O2A		2.077(2)	2.078	2.094(10)	–O3	x 2	2.086(7)	2.088	2.096(8)	2.102
–O2B		2.103(2)	2.104	2.093(10)	< M1–O >		2.084	2.086	2.096	2.100
–O3A		2.085(2)	2.085	2.097(8)						
–O3B		2.069(2)	2.069	2.069(9)						
< M1–O >		2.075	2.075	2.083						
M2–O1A		2.170(2)	2.171	2.184(9)	M2–O1	x 2	2.181(7)	2.184	2.192(7)	2.195
–O1B		2.158(2)	2.159	2.174(9)	–O2	x 2	2.097(6)	2.098	2.093(7)	2.094
–O2A		2.078(2)	2.079	2.051(10)	–O4	x 2	2.017(8)	2.024	1.997(9)	2.003
–O2B		2.097(2)	2.098	2.122(10)	< M2–O >		2.098	2.102	2.094	2.098
–O4A		1.990(2)	1.994	1.994(10)						
–O4B		2.014(2)	2.024	2.017(10)						
< M2–O >		2.084	2.087	2.090						
M3–O1A	x 2	2.077(2)	2.077	2.068(10)	M3–O1	x 4	2.087(6)	2.088	2.088(6)	2.094
–O1B	x 2	2.081(2)	2.082	2.101(10)	M3–O3	x 2	2.062(10)	2.066	2.050(12)	2.053
–O3A		2.050(2)	2.051	2.102(13)	< M3–O >		2.079	2.081	2.075	2.080
–O3B		2.039(2)	2.040	1.978(14)						
< M3–O >		2.067	2.068	2.070						
M4–O2A		2.095(2)	2.096	2.081(9)	M4–O2	x 2	2.195(8)	2.202	2.189(8)	2.192
–O2B		2.123(2)	2.123	2.144(9)	–O4	x 2	2.139(9)	2.154	2.151(10)	2.162
–O4A		2.100(2)	2.102	2.052(10)	–O6	x 2	2.672(9)	2.680	2.682(10)	2.686
–O4B		2.137(3)	2.137	2.206(11)	–O5	x 2	3.200(9)	3.206	3.216(9)	3.218
–O6A		2.487(2)	2.488	2.530(7)	$<^{[6]}$M4–O >		2.335	2.345	2.340	2.347
–O5B		2.961(2)	2.961	3.091(7)	A–O5	x 4	2.779(7)	2.779	2.778(8)	2.779
–O6B		3.017(2)	3.018	3.017(7)	A–O6	x 4	3.292(7)	3.296	3.304(8)	3.309
$<^{[5]}$M4–O >		2.188	2.189	2.202	A–O7	x 2	2.365(10)	2.370	2.361(11)	2.367
M4'–O2A		2.347(2)		2.430(9)	$<^{[6]}$A–O >		2.641	2.643	2.639	2.641
–O2B		2.258(2)		2.253(9)	$<^{[10]}$A–O >		2.901	2.904	2.905	2.908
–O4A		2.220(2)		2.126(10)	A*m*–O5	x 2	2.854(7)	2.859	2.896(8)	2.901
–O4B		2.066(3)		2.190(11)	A*m*–O5	x 2	2.792(7)	2.798	2.796(8)	2.801
–O6A		2.366(2)		2.381(8)	A*m*–O6	x 2	2.937(7)	2.942	2.864(8)	2.871
–O5B		2.747(2)		2.767(7)	A*m*–O7		2.244(10)	2.256	2.246(11)	2.255
–O6B		2.739(2)		2.706(7)	A*m*–O7		2.578(11)	2.588	2.621(11)	2.631
$<^{[5]}$M4'–O >		2.251		2.276	A*m*–O7		3.320(12)	3.327	3.215(12)	3.226
$<^{[8]}$A–O >		2.684	2.710	2.707	$<^{[8]}$A*m*–O >		2.749	2.755	2.747	2.754
O3A–H1		0.797(2)	1.303		O3–H		0.834	0.846	0.651	0.981
O3B–H2		0.773(2)	1.067							
M1–M2		3.096(1)		3.081(7)	M1–M2		3.119(3)		3.127(4)	
M1–M2		3.104(1)		3.145(7)						
O5A–O6A–O5A		189.9(1)		186.7(4)	A–A*m*		0.50(1)		0.62(1)	
O5B–O6B–O5B		158.6(1)		160.9(4)	O5–O6–O5		174.2(4)		174.5(4)	
T1A–O7A–T1A		139.1(1)		138.2(4)	T1–O7–T1		139.6(1)		139.8(1)	
T1B–O7B–T1B		135.3(1)		137.0(4)						

Table 4 Crystal 334 no. 1. Refined lattice parameters, ordering parameter ($Q_D{}^2 \propto \Sigma I_b/\Sigma I_b$), total scalar strain ($\varepsilon_{ss}$), and strain volume ($V_s$) at each annealing temperature

T (°C)	a(Å)	b(Å)	c(Å)	β (°)	V(Å^3)	$\Sigma I_b/\Sigma I_a$	ε_{ss}	V_s
30	9.697(4)	17.942(15)	5.275(4)	102.41(5)	896.3(11)	0.238	0.0041(9)	−0.0050(17)
40	9.696(4)	17.950(12)	5.275(2)	102.41(4)	896.6(8)	0.228	0.0040(8)	−0.0049(15)
50	9.700(4)	17.954(11)	5.274(2)	102.42(4)	897.0(8)	0.221	0.0042(7)	−0.0049(15)
60	9.700(4)	17.966(9)	5.279(2)	102.40(3)	898.5(7)	0.199	0.0031(7)	−0.0035(14)
70	9.699(4)	17.964(10)	5.281(2)	102.41(5)	898.6(7)	0.195	0.0030(7)	−0.0037(15)
80	9.703(4)	17.969(9)	5.281(2)	102.40(3)	899.3(7)	0.188	0.0030(7)	−0.0033(14)
90	9.704(4)	17.967(9)	5.285(2)	102.42(4)	899.9(7)	0.176	0.0026(7)	−0.0030(14)
100	9.707(5)	17.972(14)	5.282(2)	102.39(5)	900.0(9)	0.167	0.0030(8)	−0.0032(16)
110	9.710(3)	17.978(12)	5.285(3)	102.42(4)	900.9(8)	0.160	0.0027(8)	−0.0026(15)
120	9.709(4)	17.983(10)	5.285(3)	102.40(5)	901.1(7)	0.142	0.0026(7)	−0.0027(15)
130	9.710(3)	17.983(13)	5.286(2)	102.39(4)	901.4(8)	0.130	0.0025(8)	−0.0027(15)
140	9.711(4)	17.985(12)	5.287(2)	102.38(4)	901.9(8)	0.133	0.0023(7)	−0.0025(15)
150	9.712(3)	17.984(12)	5.287(2)	102.37(4)	902.0(7)	0.123	0.0024(7)	−0.0028(15)
160	9.713(3)	17.985(11)	5.289(2)	102.38(5)	902.4(7)	0.102	0.0023(7)	−0.0026(15)
170	9.715(4)	17.992(12)	5.288(2)	102.37(4)	902.9(8)	0.088	0.0023(8)	−0.0025(15)
180	9.716(4)	18.000(12)	5.290(2)	102.38(4)	903.7(8)	0.080	0.0020(8)	−0.0019(15)
190	9.716(4)	18.009(12)	5.291(2)	102.35(4)	904.4(8)	0.074	0.0016(8)	−0.0015(15)
200	9.719(4)	18.013(10)	5.293(2)	102.34(5)	905.2(7)	0.066	0.0013(7)	−0.0009(15)
210	9.718(4)	18.012(10)	5.295(2)	102.33(5)	905.5(7)	0.051	0.0010(7)	−0.0009(15)
220	9.717(4)	18.017(10)	5.297(2)	102.31(4)	906.0(7)	0.041	0.0005(7)	−0.0006(15)
230	9.719(4)	18.016(11)	5.297(2)	102.28(5)	906.3(8)	0.030	0.0007(7)	−0.0007(15)
240	9.720(4)	18.021(12)	5.299(2)	102.27(4)	907.0(8)	0.008	0.0004(8)	−0.0003(15)
250	9.720(5)	18.021(11)	5.299(2)	102.29(4)	906.9(8)	0.002	0.0005(8)	−0.0007(15)
260	9.721(4)	18.028(9)	5.300(2)	102.28(4)	907.4(6)			
270	9.722(3)	18.027(10)	5.301(3)	102.26(4)	907.9(8)			
280	9.726(4)	18.029(11)	5.302(3)	102.26(5)	908.5(9)			
290	9.727(4)	18.033(9)	5.302(2)	102.27(4)	908.8(7)			
300	9.729(5)	18.040(11)	5.302(3)	102.25(5)	909.4(9)			
310	9.729(3)	18.043(9)	5.304(2)	102.25(4)	909.9(6)			
320	9.731(3)	18.040(12)	5.303(3)	102.25(3)	909.7(9)			
330	9.733(4)	18.052(9)	5.303(3)	102.23(4)	910.6(8)			
340	9.735(4)	18.038(12)	5.303(3)	102.24(4)	910.0(8)			
350	9.735(5)	18.042(11)	5.303(3)	102.22(4)	910.3(8)			
360	9.739(3)	18.053(11)	5.304(3)	102.24(3)	911.3(8)			
370	9.736(5)	18.048(13)	5.304(2)	102.21(5)	910.8(9)			
380	9.738(4)	18.052(13)	5.306(2)	102.21(4)	911.5(8)			
390	9.737(4)	18.060(11)	5.303(1)	102.18(3)	911.5(7)			
400	9.741(5)	18.054(14)	5.307(2)	102.21(5)	912.2(9)			
410	9.744(4)	18.053(14)	5.307(2)	102.20(5)	912.4(9)			

Structural changes as a function of temperature

The main goal of this work was to understand the effect of the presence of larger cations at the B-group sites and of the A-site occupancy on the phase-transition behaviour of amphiboles. In this section, the crystal-chemical details relevant to this point are discussed, focusing on their evolution during annealing. Here, it is useful to recall that the low-T low-symmetry $P2_1/m$ structure has two independent chains of tetrahedra, whereas the high-T high-symmetry $C2/m$ structure has only one type of tetrahedral chain. The A cavity is delimited by two six-membered rings of tetrahedra belonging to two adjacent chains facing base to base. Therefore, A-site geometry and symmetry constraints are different in the two space groups. Furthermore, the coordination of the B-group cations, which connect the double chains of tetrahedra with the strip of octahedra, changes during the transition, as described below in more detail. The evolution of the structure and of the atomic displacement parameters (adp) at the A, B and O sites as a function of increasing T is summarized in Fig. 4 a, b.

Details of room T structure and cation ordering in nominal Na NaMg Mg_5 Si_8 O_{22} $(OH)_2$, are given in Iezzi et al. (2003), in which FTIR spectroscopy in the OH

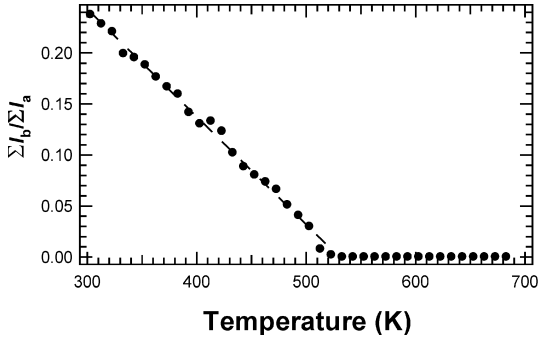

Fig. 1 Changes in the aggregate intensity ratio as a function of temperature. The *dashed line* is the polynomial fit of a 246 Landau potential to experimental data

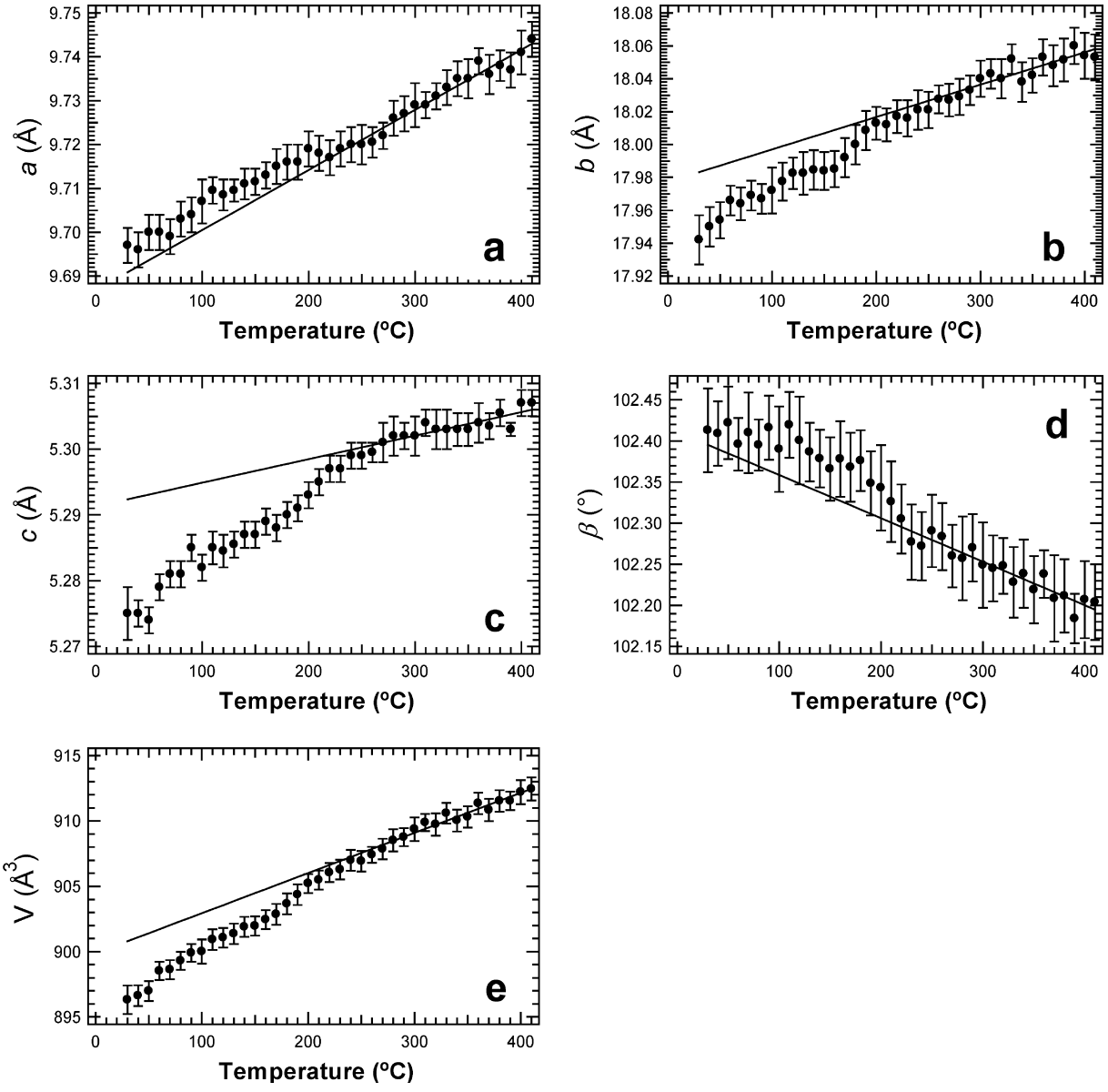

Fig. 2a–e Change in unit-cell parameters as a function of temperature. *Lines* represent extrapolation of the high temperature $C2/m$ data

region and structure refinements of samples crystallized at various P and T conditions are discussed. Iezzi et al. (2003) observed a significant decrease of the Na content in the amphibole with increasing T of synthesis. Na is equally partitioned between the A- and B-group sites, and departure from nominal end-member stoichiometry with increasing T of synthesis involves the $^{A}\square_{1}{}^{B}Mg_{1}$ $^{A}Na_{-1}{}^{B}Na_{-1}$ vector. The requirement of a proper bond strength contribution to the relevant oxygen atoms (O5, O6, O7) suggests a local coupling of the two substitutions. This feature is confirmed by the presence of a unique MgMgMg$^{A}\square$-OH absorption band falling at exactly the same wavenumber as in cummingtonite. On the contrary, no variation in the site partitioning is expected in this simplified chemical system during annealing in the investigated T range; this is confirmed by the refined site-scattering values.

Only Mg is present at the C sites in the studied sample. The pattern of octahedral mean bond lengths is M2 > M1 > M3, similar to that found in other $^{C}Mg_{5}$ $C2/m$ end members such as tremolite and richterite. This pattern is generally maintained as T increases, and also above the phase transition. On the contrary, the pattern observed in manganocummingtonite is M1 > M2 $\gg$ M3 (Sueno et al. 1972; Reece et al. 2000).

Geometrical changes in the double chains of tetrahedra are analogous to those observed in the single chains of clinopyroxenes during the $P2_1/c \rightarrow C2/c$ phase transition. Notably, the double chain of tetrahedra in the amphibole structure has fewer degrees of freedom than the single chain of tetrahedra in clinopyroxene. In fact, the sharing of one further oxygen atom

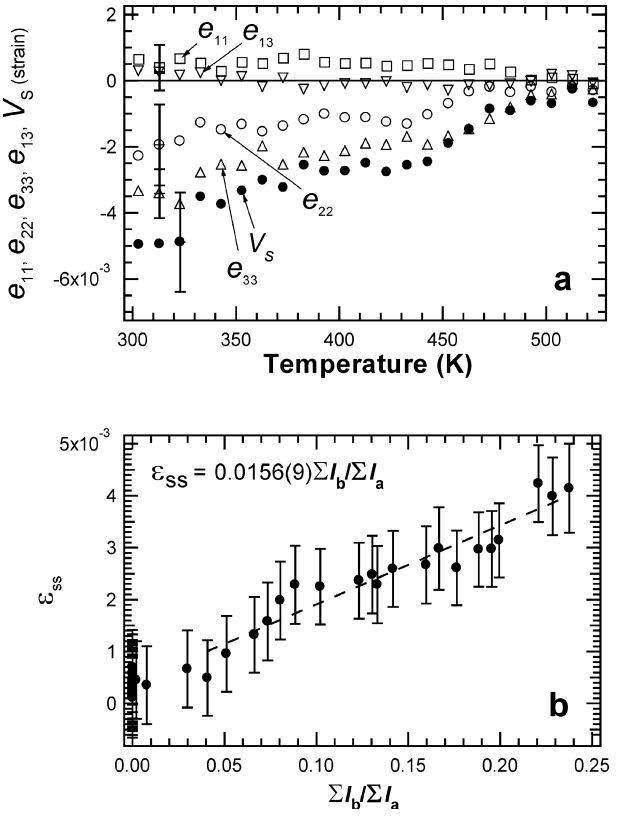

Fig. 3a Changes in the spontaneous strain components (e_{ik}) and in the volume strain (V_s) as a function of temperature. **b** Changes of the scalar strain (ε_s) as a function of the intensity ratio. *Error bars* are rather homogeneous across each series; for the sake of clarity, they are marked for only one T value

(O7), which bridges the two adjacent chains, reduces their possibility of bending and tilting (i.e. of changing the angle between the basal face of the tetrahedra and the (100) plane). The bending of the double chain along the c axis is expressed by the O5–O6–O5 angle. Figure 5 shows the evolution of O5–O6–O5 as a function of T for the sample of this work, the manganocummingtonite in Sueno et al. (1972) and the cummingtonite in Yang and Smyth (1996). In sample 334-$P2_1/m$, the A double chain is S-rotated (189.9° and 186.7°, respectively, at room T and at 413 K), and the B double chain is O-rotated (158.6 and 160.9°, respectively). In sample 334-$C2/m$, the unique double chain is O-rotated (174.2 and 174.5° at 543 and 643 K, respectively). Therefore, the A double chain first extends and then reverses its sense of rotation and shrinks, whereas the B double chain continuously extends (Fig. 5). In high-P studies, Boffa Ballaran et al. (2000) noted that the O5–O6–O5 angle is essentially independent of X_{Fe}. The manganocummingtonite studied at two different temperatures by Papike et al. (1969) and Sueno et al. (1972) has A and B double chains O-rotated at room-T, and thus the A double chain should reverse its rotation within the range 200–260 K.

The bending of the double chain along the b direction is expressed by the T1–O7–T1 angle. Boffa Ballaran et al. (2000) showed that in $C2/m$ cummingtonite T1–O7–T1 decreases with increasing P and with decreasing X_{Fe}. Comparing their data with the $P2_1/m$ data of Yang et al. (1998) these authors concluded that (1) there is an inverse correlation between the value of T1–O7–T1 averaged over the two chains, ⟨T1–O7–T1⟩, and P; (2) the $P2_1/m$ structure appears to be stable only for ⟨T1–O7–T1⟩ <142°; (3) the higher the value of this angle, the higher the pressure needed to induce the phase transition. The sample of this work has T1–O7–T1 values lower than 142° in both the $P2_1/m$ and in the $C2/m$ symmetry (Table 3), therefore this limit seems to be not valid for this composition.

A comparative analysis of the crystal-chemical database available at CNR-IGG-PV for $C2/m$ amphiboles shows that the T1–O7–T1 angle is affected by several different parameters. The most important correlations are observed with the Mg number, *mg*# (inverse), the size of the M4 site (direct) and the total A-site occupancy (direct). Comparing sample 334 with cummingtonite, the presence of Na at the A- and B-group sites should increase the T1–O7–T1 angle, whereas the absence of Fe and/or Mn should allow lower T1–O7–T1 values. This latter appears to be the most important factor, given the T1–O7–T1 value observed in the crystal of this work.

The evolution of the electron density at the A-group sites with temperature is shown in Fig. 6. There is only one A-cation position in the $P2_1/m$ symmetry, which is significantly off-centred (~0.25 Å) almost along the imaginary line joining the two farthest O7A and O7B oxygen atoms (the O7 sites are those connecting the two chains, thus forming the rings; Fig. 4a), so that there are two nearly equal short A–O7A,B distances (2.37 and 2.35 Å, respectively) and two different long A–O7A,B distances (3.62 and 3.92 Å, respectively). In the $C2/m$ symmetry, Na is ordered at the analogous Am site, and is increasingly displaced from the centre of the cavity at increasing T (0.50 and 0.62 Å, respectively, at 270 and 370 °C). Therefore, the electron density has been modelled by means of two different cation positions. Albeit this model allows a better fitting to the experimental data, the cations must locally be ordered in one of the two split positions, and not at the centre of the cavity (Hawthorne et al. 1996); therefore the A (A2/m) position is not reported in Fig. 4.

The evolution with T of the shape of the electron density at the B-group sites is shown in Fig. 7. At $T < T_c$, a split model was required for the structure refinement, with the smaller Mg in a position closer to the octahedral strip (M4 in Table 2a), and the larger Na shifted towards the double chain of tetrahedra (M4′ in Table 2a). After the transition, the electron density must be more symmetric due to the new local symmetry determined by the equivalence of the two base-facing double chains of tetrahedra. The residual elongation along the b axis does not require a split model in high-T refinements, accordingly to the stronger thermal motion. Mg changes its coordination from [5]-fold in $P2_1/m$ to [6 + 2]-fold in $C2/m$ as in analogous cummingtonites

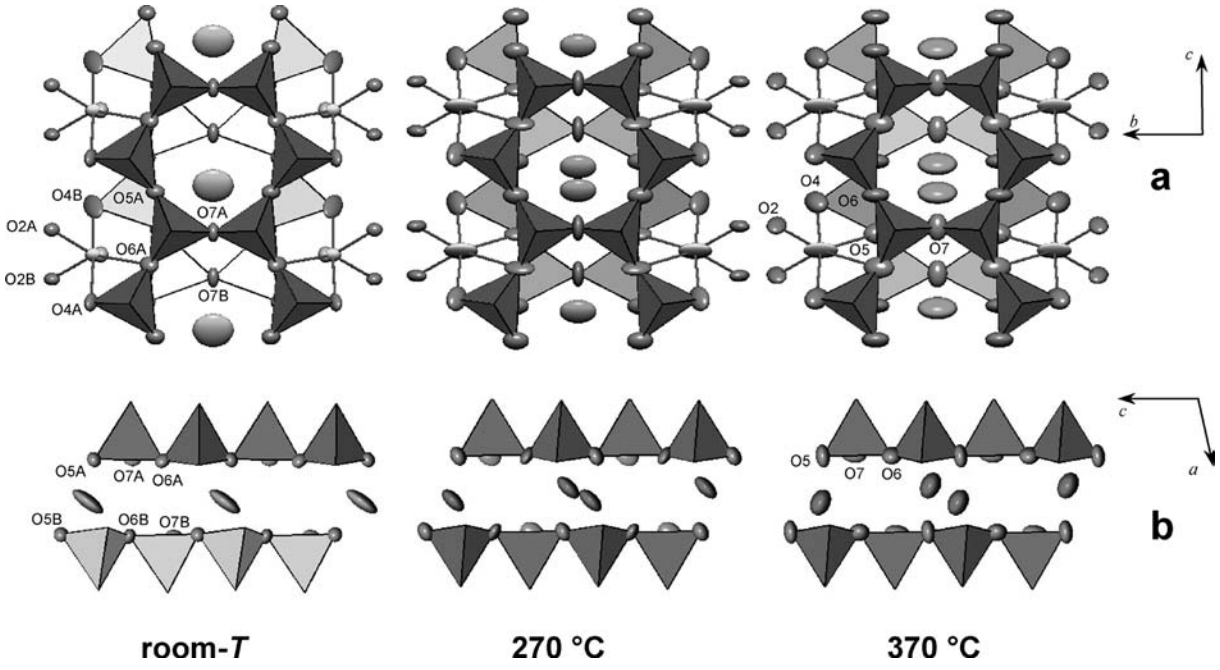

Fig. 4a–b The most relevant structure details derived from single-crystal structure refinement of sample 334. **a** Projection onto (1 0 0). **b** Projection on to (0 1 0). Ellipsoids are drawn at 95% probability. (Images made using XtalDraw written by R.T. Downs, K. Bartelmehs and K. Sinnaswamy)

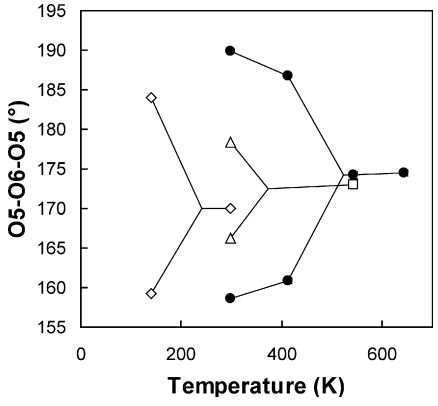

Fig. 5 Changes in the O5–O6–O5 angle as a function of temperature. *Lines* converge at T_c, and are plotted as eye guide. *Filled circles* This study; *open squares* Sueno et al. (1972); *open triangles* Papike et al. (1969); *open diamonds* Yang and Smyth (1996)

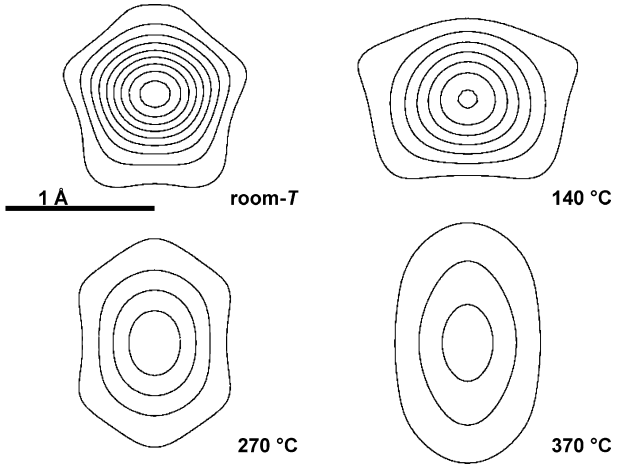

Fig. 6 The shape of the electron density at the A site in the two symmetries; projection onto (−201), *b* edge on the abscissa. Contour lines each 2 $e^{-}Å^{-3}$; first line at 2 $e^{-}Å^{-3}$

and clinopyroxenes. Na changes its coordination from [7]-fold to [6 + 2]-fold (Table 3).

The evolution of the shape of the librational ellipsoids calculated from the refined adps also deserves comment. Those observed at 270 °C, close to T_c, clearly show an intermediate behaviour between the $P2_1/m$ and the higher-T $C2/m$ structures. In particular, the adp values of the O6 and O7 oxygen atoms show preferred displacements along *b* and *c*, respectively, which are not observed at 370 °C (Fig. 4a). Also, the ellipsoids at the A site are more elongated at $T > 250$ °C (suggesting residual disorder along the direction of the main shift of the cations).

Discussion

The question to be addressed here is: why does the Na NaMg Mg_5 Si_8 O_{22} $(OH)_2$ composition, which has larger B sites and should thus simulate the behaviour of high $X_{Fe,Mn}$ cummingtonites, have $P2_1/m$ symmetry at room T, and thus higher T_c than cummingtonites?

Sueno et al. (1972) proposed that the driving force for the phase transition at the macroscopic scale is the differential expansion of the various structure moduli. Yang et al. (1998) noted different compressibilities of the B- and C-group sites compared to the T sites, the resulting mismatch being partially balanced by the stretching of the chains. Klein and Waldbaum (1967) extrapolated unit-cell parameters for □ Mg_2 Mg_5 Si_8 O_{22}

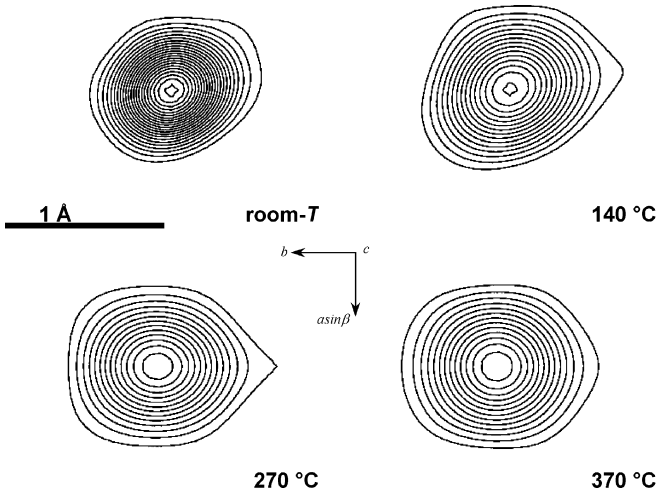

Fig. 7 The shape of the electron density at the M4 site in the two symmetries. Contour lines each 2 $e^{-}Å^{-3}$; first line at 2 $e^{-}Å^{-3}$

$(OH)_2$–$C2/m$: $a = 9.458$, $b = 17.926$, $c = 5.295$ Å and $\beta = 102.12°$. Those measured for crystal 334 no. 1 are: $a = 9.685$, $b = 17.920$, $c = 5.268$ Å and $\beta = 102.44°$. The values of the a edge and of the β angle are in the expected relation with the differences in A- and B-group site composition, respectively, because the A-site occupancy is known to lengthen the a edge, and ^{B}Na to enlarge the β angle in the amphibole structure. The values of the b and c edges would be consistent with the extrapolated values when the structural relaxation occurring during the phase transition is taken into account (cf. Fig. 2).

Yang and Hirschmann (1995) concluded that ferromagnesian cummingtonites with $X_{Mg}{}^{M4} > 0.15 \pm 0.02$, and thus an aggregate ionic radius at the M4 site ($<^{[8]}r_{M4}>$) shorter than 0.92 Å, have $P2_1/m$ symmetry at room T. Accordingly, a sample with $<^{[8]}r_{M4}> = 0.93$ Å has a T_c of 235 K (Yang and Smyth 1996) and therefore is $C2/m$ at room T. Crystal 334 no. 1 has a larger $<^{[8]}r_{M4}>$ (1.01 Å) but $P2_1/m$ symmetry at room T. Manganocummingtonites with $<^{[8]}r_{M4}> =$ 0.97 Å (Papike et al. 1969) and $<^{[8]}r_{M4}> = 0.99$ Å (Reece et al. 2000) also have $P2_1/m$ symmetry at room-T and T_c around 373 K, lower than that of this study. All three latter samples have mostly Mg at the C-group sites (> 4.80 apfu), and thus a smaller octahedral strip than the sample of Yang and Smyth (1996). It thus seems that the critical factor for the stability of the $P2_1/m$ phase actually is the relation between the aggregate ionic radii at the B- and C-group sites.

From a microscopic perspective, Boffa Ballaran et al. (2000) proposed that the driving force of the phase transition in cummingtonites is the softening of a zone-boundary vibrational mode that couples with elastic strains. The $Fe^{2+}{}_1Mg_{-1}$ solid solution does not display obvious non-ideal changes in lattice parameters which would imply small macroscopic strains associated with the phase transition (Hirschmann et al. 1994). At the microscopic level, however, strains can still be associated with the transition. Boffa Ballaran et al. (2001) provided an FTIR analysis, showed that the $P2_1/m$ phase is locally less heterogeneous than the $C2/m$ phase in Mg-rich compositions in the region of Si–O vibration, and proposed that the displacive phase transition provides a mechanism to reduce local heterogeneity.

In the crystal of this work, the presence of two geometrically different M4 sites (one occupied by Mg and one by Na) helps to reduce local strain fields, an effect which would be further enhanced by short-range ordering of ^{A}Na-^{M4}Na and $^{A}\square - {}^{M4}$Mg clusters, which is forced by bond-valence and local charge-balance requirements. Concerning the A cations, their pattern of order within the A cavity is different in the two long-range symmetries. In the $C2/m$ space group, the two distinct Am positions related by the diad are alternatively occupied along each "sandwich" of double chains running parallel to [0 0 1]. In the $P2_1/m$ space group, the position of the A cation repeats itself by translation parallel to [0 0 1] within the "sandwich", whereas adjacent "sandwiches" have A sites related by the 2_1 diad.

Acknowledgements The synthesis described in this work was done during the stay of G.I. at the Institut für Mineralogie, Universität Hannover, for which financial support was provided by an EGIDE-Ministero degli Affari Esteri Italiano fellowship. Francois Holtz, Harald Behrens and Susanne Ohlhorst of the University of Hannover are acknowledged for assistance during the synthesis. We acknowledge constructive comments by Mark Welch and an anonymous reviewer that greatly helped us to focus the results and improve the clarity of the manuscript.

References

Blessing RH, Coppens P, Becker P (1974) Computer analysis of step scanned X-ray data. J Appl Crystallogr 7: 488–492

Boffa Ballaran, T, Angel, RJ, Carpenter MA (2000) High-pressure transformation behaviour of the cummingtonite-grunerite solid solution. Eur J Mineral 12: 1195–1213

Boffa Ballaran, T, Carpenter, MA, Domeneghetti MC (2001) Phase transition and thermodynamic mixing behaviour of the cummingtonite-grunerite solid solution. Phys Chem Miner 28: 87–101

Boffa Ballaran, T, McCammon, CA, Carpenter, CA (2002) Order parameter behaviour at the structural phase transition in cummingtonite from Mössbauer spectroscopy. Am Mineral 87: 1490–1493.

Busing WR, Levy HA (1964) The effect of thermal motion on the estimation of bond lengths from diffraction measurements. Acta Crystallogr 17: 142–146

Carpenter MA, Angel, RJ, Finger LW (1990) Calibration of Al/Si order variations in anorthite. Contrib Mineral Petrol 104: 471–480

Carpenter MA, Salje EKH, Graeme-Barber A (1998) Spontaneous strain as a determinant of thermodynamic properties for phase transition in minerals. Eur J Mineral 10: 621–691

Dove MT (1997) Theory of displacive phase transitions in minerals. Am Mineral 82: 213–244.

Ghose S, Weidner JR (1972) Mg^{2+}–Fe^{2+} order–disorder in cummingtonite $(Mg,Fe)_7Si_8O_{22}(OH)_2$, a new geothermometer. Earth Planet Sci Lett 16: 346–354

Ghose S, Yang H (1989) Mn-Mg distribution in a $C2/m$ manganoan cummingtonite: crystal-chemical considerations. Am Mineral 74: 1091–1096

Hawthorne FC, Ungaretti L, Oberti R (1995) Site populations in minerals: terminology and presentation of results of crystal-structure refinement. Can Mineral 33: 907–911

Hawthorne FC, Oberti R, Sardone N (1996) Sodium at the A site in clinoamphibole: the effects of composition on patterns of order. Can Mineral 34: 577–593

Hirschmann M., Evans BW, Yang H (1994) Composition and temperature dependence of Fe–Mg ordering in cummingtonite-grunerite as determined by X-ray diffraction. Am Mineral 79: 862–877

Iezzi G, Della Ventura G, Oberti R, Cámara F, Holtz F (2003) Crystal-structure and crystal-chemistry of the synthetic $P2_1/m$ amphibole $Na(NaMg)Mg_5Si_8O_{22}(OH)_2$. Am Mineral (in press)

Klein C, Waldbaum DR (1967) X-ray crystallographic properties of the cummningtonite-grunerite series. J Geol 75: 379–392

Leake BE, Woolley AR, Arps CES, Birch WD, Gilbert MC, Grice JD, Hawthorne FC, Kato A, Kisch HJ, Krivovichev VG, Linthout K, Laird Jo, Mandarino JA, Maresh VW, Nickel EH, Rock NMS, Schumacher JC, Smith DC, Stephenson NN, Ungaretti L, Whittaker EJW, Youzhi G (1997) Nomenclature of amphiboles: report of the subcommittee on amphiboles of the International Mineralogical Association, Commission on New Minerals and Mineral Names. Am Mineral 82: 1019–1037

Lehmann MS, Larsen FK (1974) A method for location of the peaks in step-scan-measured Bragg reflections. Acta Crystallogr (A) 30: 580–584

North ACT, Phillips DC, Mathews FS (1968) A semi-empirical method of absorption correction. Acta Crystallogr (A) 30: 580–584

Oberti R, Ottolini L, Della Ventura G, Prella D (2000) Excess OH in amphiboles: a structural model obtained by combining structure refinement, complete chemical characterization, and FTIR spectroscopy. Plinius 24: 157. Plinius is the Halian Supplement of the European Journal of Mineralogy – The reference quoted is an abstract

Papike JJ, Ross M, Clark JR (1969) Crystal-chemical characterization of clinoamphiboles based on five new structure refinements. Mineral Soc Am Spec Pap 2: 117–136

Prewitt CT, Papike JJ, Ross M (1970) Cummingtonite: a reversible, non quenchable transition from $P2_1$/m to $C2/m$ symmetry. Earth Planet Sci Lett 8: 448–450

Reece JJ, Redfern T, Welch MD, Henderson CMB (2000) Mn–Mg disordering in cummingtonite: a high temperature neutron powder diffraction study. Miner Mag 64: 255–266

Sheldrick, GM (1997) SHELX-97, program for crystal structure determination. University Göttingen, Germany

Sueno S, Papike JJ, Prewitt CT, Brown GE (1972) Crystal chemistry of high cummingtonite. J Geophys Res 77: 5767–5777

Yang H, Hirschmann MM (1995) Crystal structure of $P2_1/m$ ferromagnesian amphibole and the role of cation ordering and composition in the $C2/m$–$P2_1/m$ transition in cummingtonite. Am Mineral 80: 916–922

Yang H, Smyth JR (1996) Crystal structure of $P2_1/m$ ferromagnesian cummingtonite at 140 K. Am Mineral 81: 363–368

Yang H, Hazen RM, Prewitt CT, Finger LW, Lu R, Hemley RJ (1998) High-pressure single-crystal X-ray diffraction and infrared spectroscopic studies of the $C2/m \rightarrow P2_1/m$ phase transition in cummingtonite. Am Mineral 83: 288–299

Zhang L, Ahsbahs H, Kutoglu A, Hafner SS (1992) Compressibility of grunerite. Am Mineral 77: 480–483